



HAL
open science

Successive steps of growth of compacted graphite in cast irons

Jon Sertucha, Jacques Lacaze, Anna Regordosa, Urko de La Torre

► **To cite this version:**

Jon Sertucha, Jacques Lacaze, Anna Regordosa, Urko de La Torre. Successive steps of growth of compacted graphite in cast irons. *Tecnologia em Metalurgia, Materiais e Mineração*, 2022, 19, pp.e2620. 10.4322/2176-1523.20222620 . hal-03689079

HAL Id: hal-03689079


<https://hal.science/hal-03689079v1>

Submitted on 19 Jul 2022

HAL is a multi-disciplinary open access archive for the deposit and dissemination of scientific research documents, whether they are published or not. The documents may come from teaching and research institutions in France or abroad, or from public or private research centers.

L'archive ouverte pluridisciplinaire **HAL**, est destinée au dépôt et à la diffusion de documents scientifiques de niveau recherche, publiés ou non, émanant des établissements d'enseignement et de recherche français ou étrangers, des laboratoires publics ou privés.

Successive steps of growth of compacted graphite in cast irons

Jon Sertucha¹
Jacques Lacaze^{2*} 
Anna Regordosa¹
Urko de la Torre¹

Abstract

Holding during 8 hours a melt prepared for casting SGI leads to fading of the spheroidizing treatment and thus to growth of compacted graphite instead of spheroidal graphite. Such a melt was cast in thermal analysis cups at 25-30 minutes interval without inoculation. It solidified first in the stable system and more and more in the metastable system. Accordingly, recalcence first increased as more of compacted graphite solidified, but then decreased when more and more of the solidification occurred in the metastable system. Comparison of the results of the present study with those of a previous similar series showed a higher peak recalcence while the number of compacted graphite cells and the graphite fraction were the same within experimental scattering. Furthermore, as the amount of spheroidizers was similar in both series, there is no clear reason for this difference in recalcence, which should be investigated further.

Keywords: Cast-iron; Compacted graphite; Solidification.

1 Introduction

Since the 1980's, a wealth of research works have dealt with growth of compacted graphite as it was realized that compacted graphite irons (CGI) were going to provide a better alternative to lamellar cast irons (LGI) for diesel engines. However, this is only in the mid of the 1990's that the challenge was considered by industries, and Tupy in Brazil was the first company to make the step with the support of the Sintercast process control system.

Ensuring that at least 80% of the graphite will be compacted and the remaining 20% will be spheroidal means that an acute balance between sulfur and “anti-spheroidizing” elements, on the one hand, and spheroidizing elements, on the other hand, is achieved. That the world production of CGI castings is strongly increasing at present time demonstrates this goal has been reached.

Achieving the above mentioned balance does not mean that the amount of elements acting on graphite shape is always the same. Indeed, a few works have demonstrated that the shape of the compacted graphite can change with the amount of free sulfur. Wilson Guesser was certainly amongst the first to realize that this could affect the mechanical properties of the material [1] and to illustrate it, see Figure 1: the tiny changes between the two CGI illustrated in the figure lead to definite change in the mechanical properties that can be related to the difference in the sharpening of the graphite tips.

One may wonder if the compacted graphite that is obtained is the same when adding Mg to a desulfurized melt, as in the Sintercast process, or adding sulfur to a fully

spheroidized melt as patented by Menk and Brandenberger [2]. Bazdar et al. [3] investigated the transition from spheroidal graphite (SG) to compacted graphite (CG) and then to lamellar graphite (LG) by adding sulphur to a melt containing 0.057 wt.% Mg. The graphite shape was characterized by the aspect ratio, AR, i.e. the ratio of graphite length by graphite width, and the transition between the various graphite shapes was quantified. In this work, the ultimate tensile strength (UTS) varied from 370 MPa to 220 MPa when the aspect ratio increased from 10 to 25, stressing the need to master compacted graphite shape.

Understanding why and how compacted graphite can change requires following its formation during the whole solidification process. As a first step in this line, a study using quenching at various times during solidification of a melt leading to compacted graphite was carried out. These experiments and the conclusions drawn from the microstructure observation are presented here.

2 Experimental details

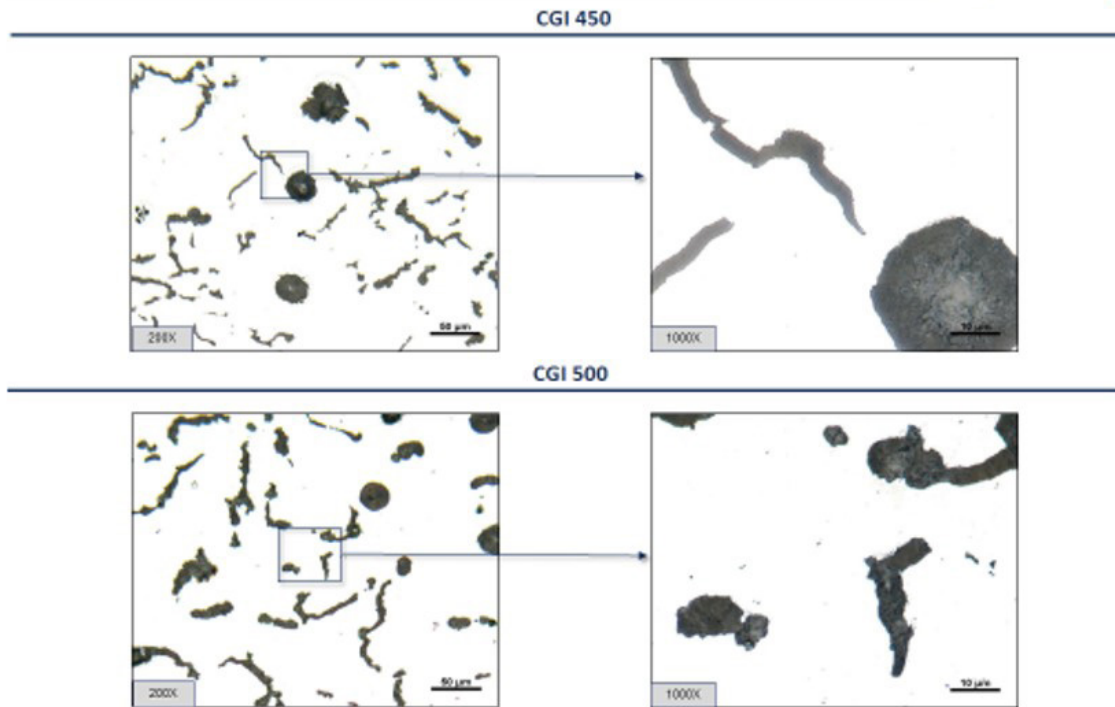
All the experimental procedure has been detailed previously [4]. In this previous work, casting of thermal analysis (TA) cups was performed using a melt maintained in a 4 tons pressurized pouring unit with a nitrogen atmosphere. The original melt had been prepared for casting spheroidal graphite iron (SGI) parts, and holding it four 8 hours led to fading of the spheroidizing

¹AZTERLAN, Basque Research Technological Alliance, Durango, Spain.

²CIRIMAT, Université de Toulouse, Toulouse, France.

*Corresponding author: jacques.lacaze@ensiacet.fr





32

Figure 1. Effect of shape of compacted graphite on the CGI properties, CGI-450 (top row) and CGI-500 (bottom row). Courtesy W. Guesser.

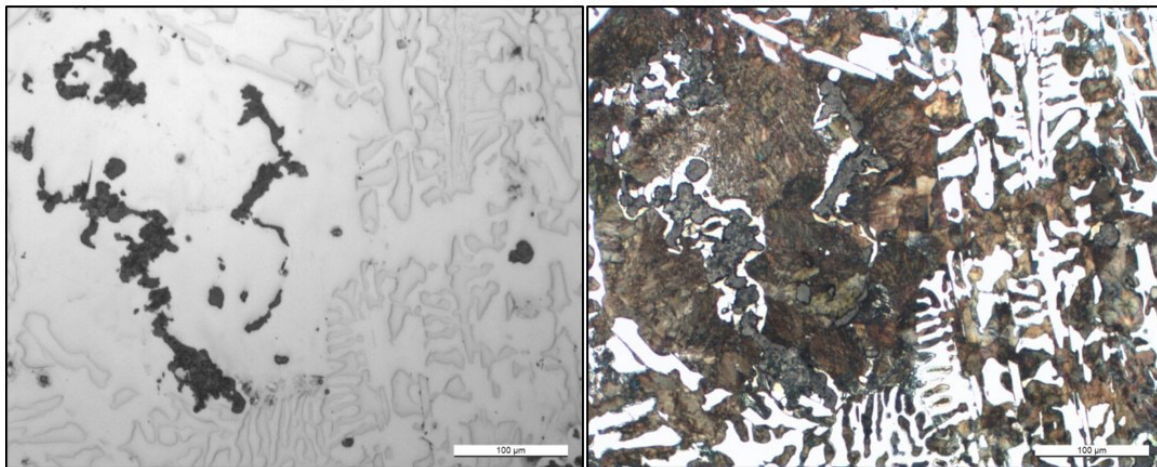


Figure 2. Micrograph of the same area before and after etching showing a CG cell surrounded by metastable eutectic.

treatment. Three TA cups were poured every 25-30 min, with 0.02 wt.% and 0.10 wt.% addition of inoculant at the bottom of the two first cups and without any inoculant addition in the third one. A medal was cast also for chemical analysis.

A section close to the thermocouple junction of the TA cups was prepared for metallographic inspection. After grinding and polishing, metallographic analysis was carried out using light optical microscopy before and after etching with Nital 5% as illustrated with the micrographs in Figure 2. The morphology and characteristics of graphite

were analysed on the unetched sections while CG cells trapped within white eutectic could be evidenced on the etched sections. These observations showed a transition from SG to CG as already observed by Liu et al. [5] and Dioszegi et al. [6,7] who studied the change from SGI to CGI and then to LGI by holding a given melt for various length of time. For not-inoculated alloys, the transition of the graphite shape was most rapid and associated with more and more of the solidification occurring in the metastable system [8].

Table 1. Chemical composition range of the 18 samples

C	Si	Mn	P	S	Mg	Ce	La	Ti
3.73-3.84	2.33-2.37	0.56-0.57	0.024-0.029	<0.005	0.003-0.024	0.0100-0.0012	0.0025-0.0002	0.023-0.025

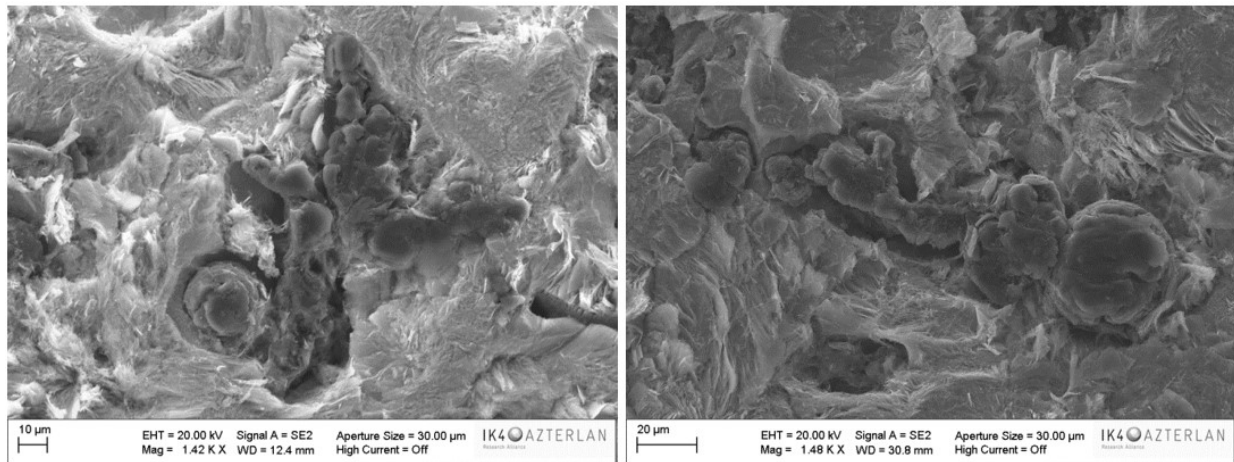


Figure 3. Scanning electron micrographs of deep etched samples of the first series showing protuberances having developed from graphite spheroids.

Deep etching of the samples of the previous series evidenced graphite spheroids with protuberances developing outwards [8] as illustrated with the micrographs in Figure 3. These observations suggested carrying out a second series of experiments where solidification of some selected TA cups could be interrupted by quenching. This second series of castings followed the same procedure as for the first series. 18 castings were performed during a holding time of 8 h, and five quenching experiments were performed as described in the following section. For the present study, only the non-inoculated samples will be considered. The range of chemical composition of the samples in this series of castings as measured on the medals is shown in Table 1.

3 Results

Figure 4 shows the evolution with holding time of the chemical composition of the cast samples. It is seen that the silicon remained nearly constant at 2.37-2.33 wt.% while the carbon content slightly decreased from 3.84 to 3.73 wt.%. Thus, the carbon equivalent CE calculated with the CE_{99} expression previously detailed [4] also decreased. As expected, there was a marked fading of the spheroidizing treatment as shown with the decrease of Mg, Ce and La contents.

To this evolution of melt composition corresponds an evolution of the cooling curves. In Figure 5 are plotted four of them, corresponding to the first and last samples of the series (#1 and #18, respectively) and two intermediate samples. A micrograph has been added for each sample that

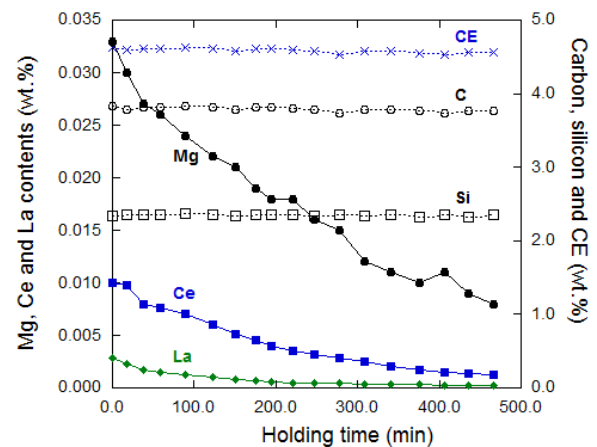


Figure 4. Evolution of the content in the most important elements during holding of the melt. CE stands for carbon equivalent.

illustrates the evolution of graphite shape. Sample #1 shows a SGI microstructure and a eutectic plateau at a temperature characteristic of a fully stable solidification. As the holding time increased, the minimum temperature before the eutectic plateau decreased and the microstructure was observed to contain more and more of compacted graphite. The micrograph for sample #6 shows that a few large spheroids were still present, but most of the eutectic solidification involved compacted graphite so that recalescence was significant. As the time elapsed further, the graphite fraction was found to decrease, meaning that a significant part of the eutectic reaction processed in the metastable system with lower or no recalescence. This is what is seen with the flat eutectic

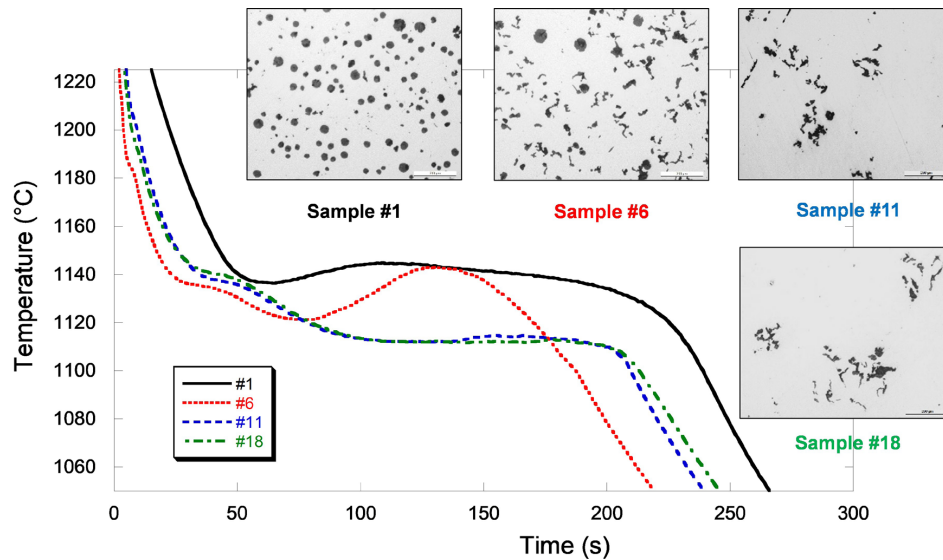


Figure 5. Cooling curve of selected samples and associated micrographs.

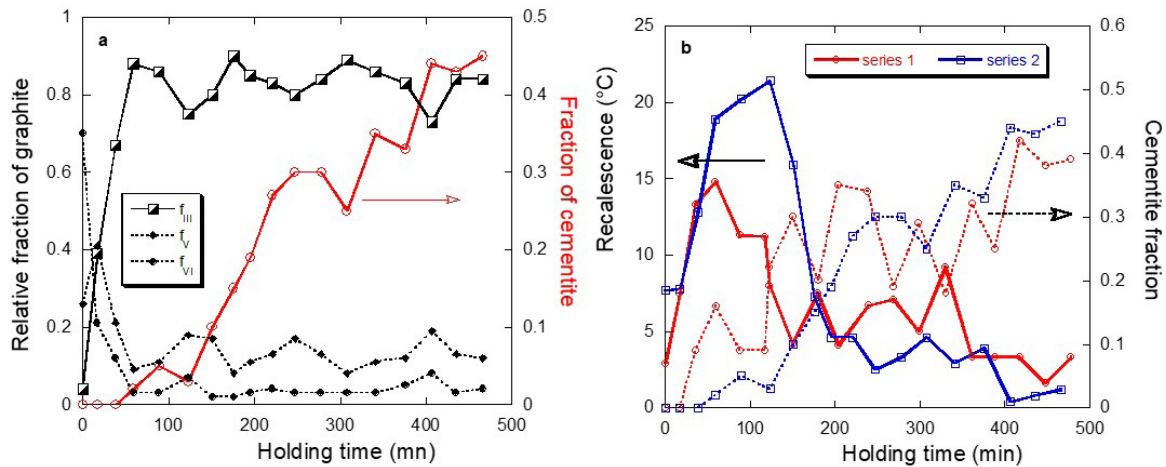


Figure 6. (a) Evolution of graphite distribution and amount of cementite as function of holding time; (b) Correlation between recalescence (solid lines) and cementite fraction (dotted lines) for the previous (red) and present (blue) series of castings.

plateau of the second intermediate sample #11 and for the last sample #18.

The graphite distribution was characterized by classifying graphite particles in class III (compacted), V and VI (spheroids). The relative amount of each class is plotted as function of holding time in Figure 6a where it is seen that the maximum in class III is reached at the same time as the minimum in classes V and VI. It is worth noting however that some spheroids remained present all the along the series of casting.

Figure 6a shows also that cementite appeared in casting #4 in an amount that then increased continuously until the end of the experiments. In the analysis of the first series [4], this behavior could be correlated with a continuous decrease of the number of graphite particles and the same could be noticed in the present study. Figure 6b shows the

evolution of the recalescence and of the cementite fraction. As compacted graphite appears and becomes more and more prevalent, recalescence increases even when some cementite appears. However, with the decrease of the number of CG cells the associated rate of heat release and thus recalescence both decrease, while solidification in the metastable system is favored. This analysis is supported by the comparison of the results for the first series and the present one in Figure 6b.

Because of the dramatic decrease of the minimum temperature before the eutectic reaction, the question that has often been raised is if there are any graphite particles present during the pre-eutectic solidification event, i.e., before the eutectic plateau. That this is so was postulated when modelling CG solidification, but it was considered that the coupled growth of graphite and austenite that gives rise to recalescence needs high undercooling. It has been proposed

that this delay in the establishment of the coupling occurs because of branching limitation of compacted graphite when compared to lamellar graphite [9]. It was considered however of interest to verify this claim by quenching samples during the pre-eutectic arrest and early during the eutectic arrest. The five quenching experiments that have been carried out are illustrated in Figure 7 where are plotted the cooling curves just before and just after each of the quenching tests.

What is seen in Figure 7 is that both spheroids more than 10 μm in diameter and austenite dendrites co-exist at the beginning of the pre-eutectic arrest. This is only in the middle of this pre-eutectic arrest that compacted graphite could be observed. In contradistinction, only CG cells are seen in samples quenched during the early stage of the eutectic plateau, meaning the spheroids mentioned above got included in these CG cells. To complement these observations, Figure 8 shows micrographs of two quenched samples after etching that reveals the evolution of the graphite particles embedded in quenched ex-austenite transformed to martensite.

4 Discussion

The present results do confirm that graphite precipitation in CGI starts with spheroidal graphite as in SGI as reported by Pan et al. [10]. An interesting way of demonstrating this was by observing spheroidal graphite flotation in hyper-eutectic CGI [10,11]. During cooling and after some time of spheroidal growth, protuberances appear on the spheroids which lead to the development of two-phase austenite compacted graphite eutectic cells [10].

In agreement again with Pan et al. [10], it has effectively been confirmed here that CG growth starts before the eutectic plateau though to a quite limited extent. As growth of CG relates to a two-phase austenite-graphite growth, a parallel could be made with LGI solidification and solidification of CGI could be modelled assuming a low branching of graphite protuberances [9]. Because of this low branching capability, this is only when a high undercooling with respect to the stable eutectic temperature has been reached that growth of CG cells becomes significant as observed here with the samples quenched during the early stage of the eutectic plateau. However, when coupled growth has started at this high undercooling, it leads to the marked recalescence which is so characteristic of CGI solidification unless metastable solidification competes successfully with the stable one.

That graphite in CG cells is interconnected has long been evidenced and the question arose of the possibility of having neighboring cells merging during solidification. This would look weird because of the associated development of microsegregation but it was noticed by Pan et al. [10] and has been reported recently based on X-ray tomography of samples quenched during solidification [12] as well as by in-situ tomography [13]. As a matter of fact, such a merging is highly unlikely in the present study because most of the CG cells got surrounded by white eutectic while they were still at an early growth stage.

The results of the present study have been compared to those of the previous series of castings and it could be noticed in Figure 6b a significant difference between the maximum recalescence values. The first idea would have been that the graphite fraction of the two series differed

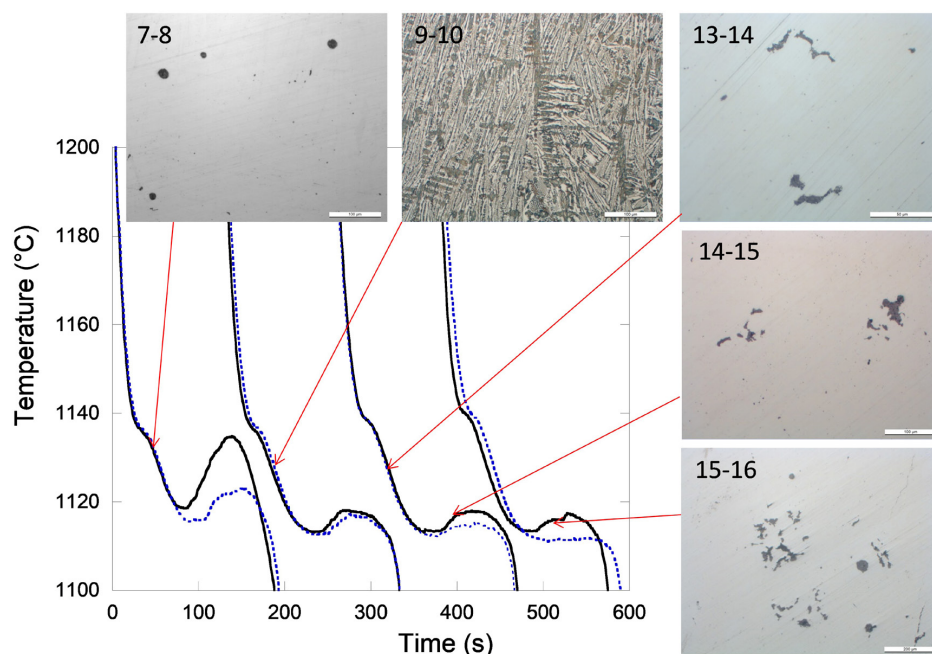


Figure 7. Cooling curves recorded before and after each of the five quenching tests, and typical micrograph of each quenched sample. The cooling curves have been shifted along the time axis for readability. The arrows point to the time during cooling at which quenching was performed.

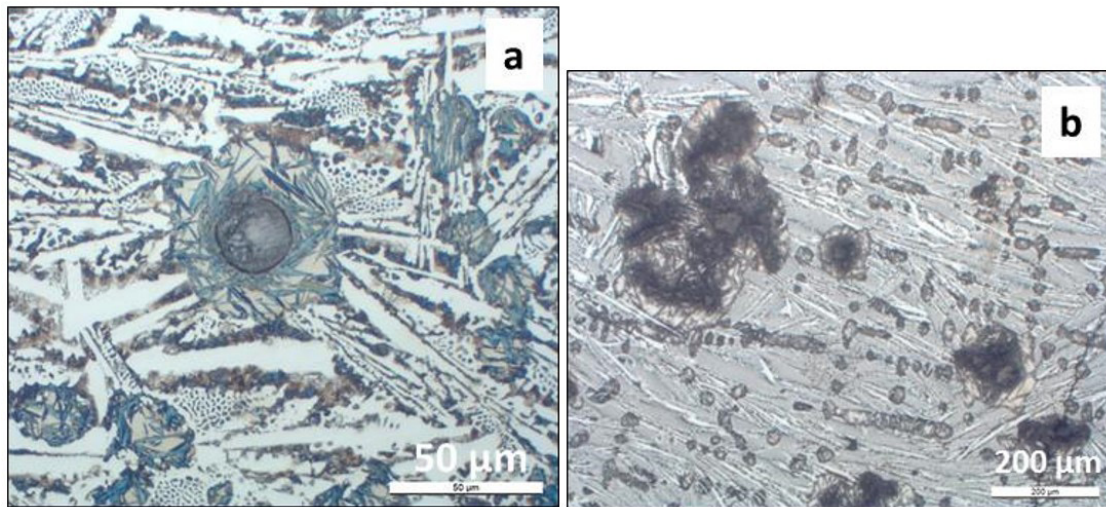


Figure 8. Example of graphite particles in the first (a) and last (b) quenched samples.

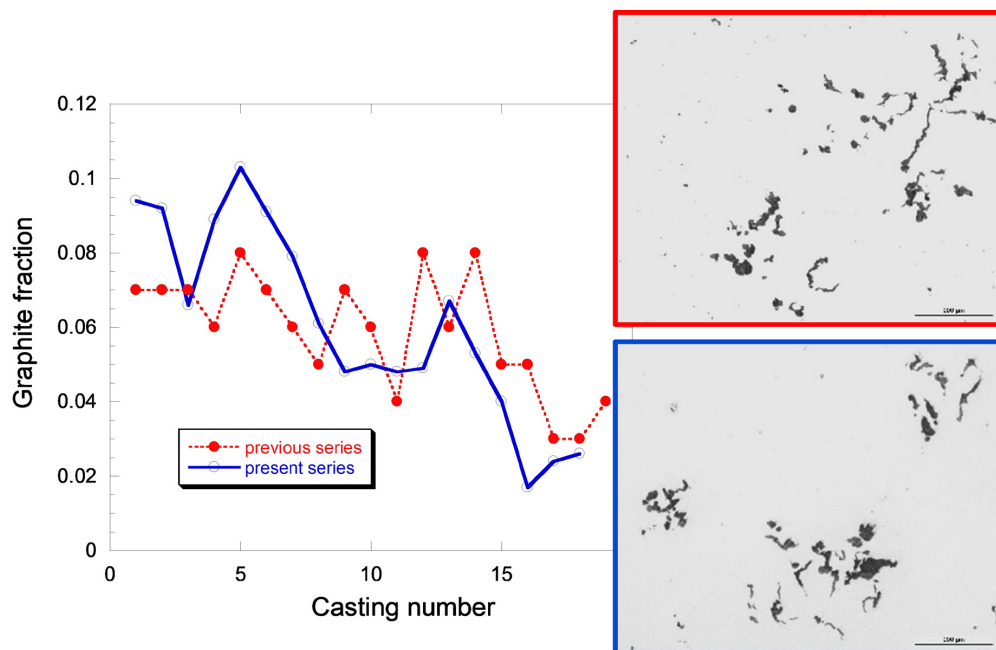


Figure 9. Comparison of the evolution of the graphite fraction between the two series of castings with a micrograph of the casting #13 of each one.

significantly. However, Figure 9 shows a comparison of the evolution of the graphite fraction in the two series of castings and it is seen they are quite similar. A micrograph of the casting #13 of each series has been added whose comparison suggests a difference in the size of the cells.

The number of CG cells was thus evaluated and found very similar to the number previously reported [4] as shown with Figure 10a. However, it was noticed that the average size of the five largest cells in each sample were far larger in the first series of castings than in this work. As the graphite fraction is nearly the same in both castings (Figure 9), this would mean that the worms were thinner in the former work than they are in the present one. Validating

this conclusion would require a statistical analysis on a large number of micrographs.

A possible reason for explaining the size difference could be melt chemistry. Figure 10b shows the change in the Mg, Ce and La content in both series during the whole holding time. The values are close to each other, though all slightly larger for the first series. Stefanescu et al. [14] reported that an increase in compacting elements (Mg and rare earths) generally increases the thickness of the worms, which seems opposite to the present finding. This difference between these two studies may be due to the fact that the samples studied by Stefanescu et al. [14] solidified in the stable system while our procedure caught the CG cells

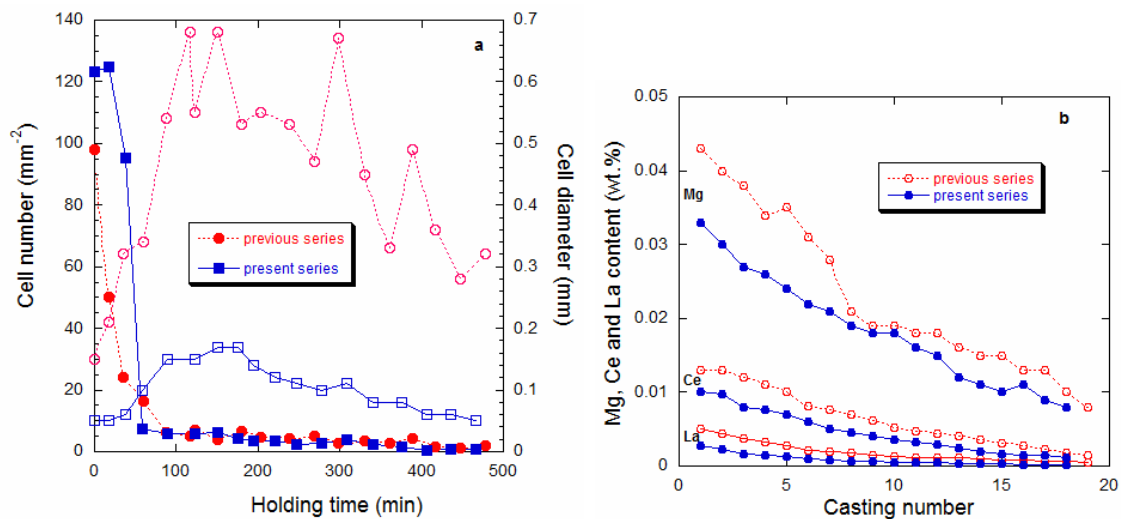


Figure 10. (a) Evolution of the cell number (solid symbols) and cell size (open symbols) for the previous (red) and present (blue) series of castings; (b) Change in the content of Mg, Ce and La during the holding of both series.

while growing. This means that a significant part of graphite precipitation might occur behind the solidification front by solid-state diffusion of carbon from the remaining liquid through austenite. Yet, the relation with recalescence is not straightforward and needs further investigation.

5 Conclusion

Holding during 8 hours a melt prepared for casting SGI leads to fading of the spheroidizing treatment and thus to growth of compacted graphite instead of spheroidal

graphite. If the melt is cast without inoculation, the number of graphite nuclei decreases with increasing holding time and the cooling curves show higher and higher undercooling, associated with a recalescence that first increases and then decreases when metastable solidification takes over.

Comparison of the results of the present study with those of a previous similar series showed a higher peak recalescence while the number of CG cells and the graphite fraction were the same within experimental scattering. There is no clear reason for such a difference and this needs to be studied further.

References

- 1 Guesser WL, Martins LPR. Stiffness and vibration damping capacity of high strength cast irons. SAE Technical Papers. 2016;25:36-0126.
- 2 Menk W, Brandenberger U. Process for manufacturing cast iron containing vermicular graphite. United States patent US 4,900,509, 1990.
- 3 Bazdar M, Abbasi HR, Yaghtin AH, Rassizadehghani J. Effect of sulfur on graphite aspect ratio and tensile properties in compacted graphite irons. Journal of Materials Processing Technology. 2009;209:1701-1705.
- 4 Regordosa A, de la Torre U, Sertucha J, Lacaze J. Quantitative analysis of the effect of inoculation and magnesium content on compacted graphite irons: experimental approach. Journal of Materials Processing Technology. 2020;9:11332-11343.
- 5 Liu J, Yi L, Li G, Liu C, Li Y, Yang Z. Influence of fading on characteristics of thermal analysis curve of compacted graphite iron. China Foundry. 2011;8:295-299.
- 6 Hernando JC, Domeij B, Gonzalez D, Amieva JM, Dioszegi A. New experimental technique for nodularity and Mg fading control in compacted graphite iron production on laboratory scale. Metallurgical and Materials Transactions. A, Physical Metallurgy and Materials Science. 2017;48:5432-5441.
- 7 Domeij B, Hernando JC, Dioszegi A. Size distribution of graphite nodules in hypereutectic cast irons of varying nodularity. Metallurgical and Materials Transactions. B, Process Metallurgy and Materials Processing Science. 2018;49:2487-2504.

- 8 Regordosa A, de la Torre U, Loizaga A, Sertucha J, Lacaze J. Microstructure changes during solidification of cast irons - Effect of chemical composition and inoculation on competitive spheroidal and compacted graphite growth. *International Journal of Metalcasting*. 2020;14:681-688.
- 9 Lacaze J, Regordosa A, Sertucha J. Quantitative analysis of the effect of inoculation and magnesium content on compacted graphite irons: a modelling approach. *ISIJ International*. 2021;61:1539-1549.
- 10 Pan EN, Ogi K, Loper CR. Analysis of the solidification process of compacted/vermicular graphite cast iron. *AFS Transactions*. 1982;90:509-527.
- 11 Sun GX, Loper CR. Influence of hypereutectic graphite on the solidification of gray cast iron. *AFS Transactions*. 1983;91:217-224.
- 12 Shi GQ, Yang Z, Li JP, Tao D, Ma ZJ. Investigation on the graphite nucleation and growth mechanism of the compacted graphite iron. *Journal of Materials Processing Technology*. 2020;9:8186-8196.
- 13 Xu C, Wigger T, Azeem MA, Andriollo T, Fæster S, Clark SJ, et al. Unraveling compacted graphite evolution during solidification of cast iron using in-situ synchrotron X-ray tomography. *Carbon*. 2021;184:799-810.
- 14 Stefanescu DM, Loper CR, Voigt RC, Chen IG. Cooling curve structure analysis of compacted/vermicular graphite cast irons produced by different melt treatments. *AFS Transactions*. 1982;90:333-348.

Received: 20 July 2021

Accepted: 22 Oct. 2021